nature neuroscience

Asynchronous GABA release generates long-lasting inhibition at a hippocampal interneuron–principal neuron synapse

Stefan Hefft & Peter Jonas

Hippocampal GABAergic interneurons show diverse molecular and morphological properties. The functional significance of this diversity for information processing is poorly understood. Here we show that cholecystokinin (CCK)-expressing interneurons in rat dentate gyrus release GABA in a highly asynchronous manner, in contrast to parvalbumin (PV) interneurons. With a gamma-frequency burst of ten action potentials, the ratio of asynchronous to synchronous release is 3:1 in CCK interneurons but is 1:5 in parvalbumin interneurons. N-type channels trigger synchronous and asynchronous release in CCK interneuron synapses, whereas P/Q-type Ca^{2+} channels mediate release at PV interneuron synapses. Effects of Ca^{2+} chelators suggest that both a long-lasting presynaptic Ca^{2+} transient and a large distance between Ca^{2+} source and sensor of exocytosis contribute to the higher ratio of asynchronous to synchronous release in CCK interneuron synapses. Asynchronous release occurs at physiological temperature and with behaviorally relevant stimulation patterns, thus generating long-lasting inhibition in the brain.

The hippocampus is a complex neuronal network that encodes sequences of places and events[1]. Inhibitory interneurons control fundamental aspects of the function of this network by means of their GABAergic output synapses[2,3]. The subcellular location of the synapses and the time course of the inhibitory conductance are important determinants of the functional impact of a given interneuron on its target cells. Somatic GABA synapses control action potential discharge, whereas dendritic GABA synapses control local electrogenesis and synaptic plasticity[4]. Fast 'phasic' synapses synchronize the activity of principal cell ensembles and contribute to the generation of high-frequency oscillatory activity in interneuron networks[5,6], whereas slow 'tonic' inhibition may set the gain or offset of the input-output relations of postsynaptic target cells[7,8].

Most synapses in the PNS and CNS release transmitter in a tightly synchronized manner after a presynaptic action potential[9,10]. This especially holds for the output synapses of PV interneurons, a major class of interneuron in cortical circuits[11–13]. However, there are also examples of asynchronous transmitter release at both excitatory and inhibitory synapses in culture[14–16]. Furthermore, asynchronous release has been found in excitatory parallel fiber–stellate cell synapses in juvenile rat cerebellum[17] and in inhibitory synapses in the nucleus magnocellularis of chick auditory system[18]. The contribution of asynchronous release to synaptic transmission is minor under physiological conditions, but it can be enhanced by substitution of external Ca^{2+} with Sr^{2+} (refs. 14,19,20).

If cortical inhibitory synapses were capable of asynchronous release, they could generate a fluctuating and long-lasting inhibitory signal ideally suited for the purpose of gain control in postsynaptic target cells[7]. However, whether asynchronous release occurs at inhibitory synapses in the mature cortex under physiological conditions has not yet been determined. We addressed this issue in the dentate gyrus, where different interneuron subtypes are clearly defined[2].

RESULTS

Axonal arborization of CCK and PV interneurons

To examine the functional properties of GABAergic synapses formed by identified types of interneurons, we made paired recordings between interneurons and granule cells in the dentate gyrus. Pre- and postsynaptic neurons were filled with biocytin during recording and labeled with Alexa 488–conjugated avidin. The subtype of the presynaptic interneuron was determined by immunocytochemistry with primary antibodies against either CCK or PV and secondary Alexa 568–conjugated antibodies. Confocal stacks of a CCK interneuron–granule cell pair (**Fig. 1a**) and a PV interneuron–granule cell pair (**Fig. 1b**) show that the axon of the CCK interneuron was mainly located in the inner molecular layer, whereas the axon of the PV interneuron was almost exclusively located in the granule cell layer. Similar results were obtained in all synaptically connected interneuron–granule cell pairs examined (15 CCK and 21 PV interneuron–granule cell pairs). Thus, in the dentate gyrus, CCK interneurons innervate mainly the

Physiologisches Institut der Universität Freiburg, Hermann-Herder-Str. 7, D-79104 Freiburg, Germany. Correspondence should be addressed to P.J. (peter.jonas@physiologie.uni-freiburg.de).

Received 16 June 2005; accepted 19 August; published online 11 September 2005; doi:10.1038/nn1542

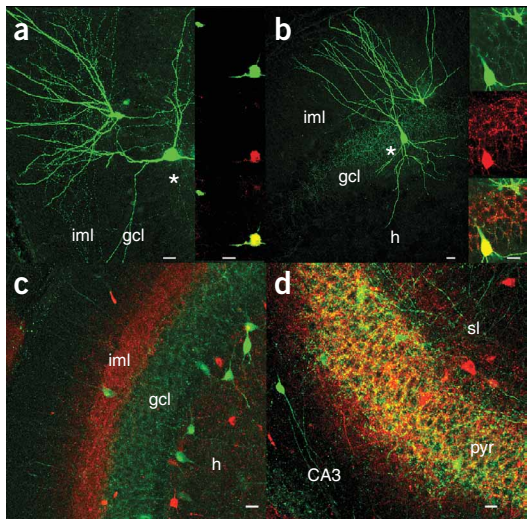

Figure 1 CCK- and PV-positive interneurons in the dentate gyrus have adjacent, but largely non-overlapping, axonal arborizations. (**a**,**b**) Confocal stacks of pairs of a presynaptic interneuron (asterisk) and a postsynaptic granule cell both filled with biocytin and stained with Alexa 488-conjugated avidin. In **a**, the presynaptic interneuron was identified as CCK-positive by immunocytochemistry (insets: top, Alexa 488–conjugated avidin; center, anti-CCK primary, Alexa 568–conjugated secondary antibody; bottom, overlay). In **b**, the presynaptic interneuron was identified as PV-positive (insets: top, Alexa 488–conjugated avidin; center, anti-PV primary, Alexa 568–conjugated secondary antibody; bottom, overlay). Note the different location of the axonal arborization (inner molecular layer (iml)) for the CCK interneuron in **a** versus granule cell layer (gcl) for the PV interneuron in **b**. (**c**,**d**) Double labeling of CCK immunoreactivity (Alexa 568; red) and PV immunoreactivity (Alexa 488, green) in the dentate gyrus (**c**) and the CA3 region (**d**). CCK and PV immunoreactivities were separated in the dentate gyrus (CCK in the inner molecular layer and PV in the granule cell layer) but largely overlapped in the CA3 region (in the pyramidal cell layer) (pyr)). h, hilus; sl, stratum lucidum. Scale bars, 20 μm.

proximal dendrites, whereas PV interneurons innervate primarily the perisomatic region of granule cells.

The spatial segregation of the axons of CCK and PV interneurons in the dentate gyrus seemed to be in contrast to previous findings in the hippocampal CA3 and CA1 region, where both CCK- and PV-positive interneurons innervate the perisomatic domain of pyramidal cells[21–23]. To compare the location of axons of the two types of interneurons among the hippocampal subfields, we performed double immunolabeling for CCK and PV (**Fig. 1c**,**d**). In the dentate gyrus, CCK-positive axon terminals formed a band in the inner molecular layer, whereas PV-positive axon terminals were largely confined to the granule cell layer (**Fig. 1c**). In contrast, in both the CA3 (**Fig. 1d**) and the CA1 subfields, CCK- and PV-positive terminals extensively overlapped in the perisomatic region.

Differences in basic release properties

We next compared the functional properties of GABA release from immunocytochemically identified CCK and PV interneuron–granule cell synapses in paired recordings (**Fig. 2**). Unitary inhibitory postsynaptic currents (IPSCs) were evoked by applying brief current pulses to the presynaptic neuron. CCK interneuron–granule cell synapses differed from PV interneuron–granule cell synapses in several basic properties of transmitter release. First, CCK interneuron–granule cell synapses showed a significantly longer synaptic latency than PV interneuron–granule cell synapses (3.60 ± 0.39 ms versus 1.84 ± 0.08 ms; $P < 0.001$; 14 and 21 pairs, respectively; 22 ± 2 °C; **Fig. 2a–c**). Second, transmitter release was less precisely timed in CCK than in PV interneuron output synapses, consistent with previous observations in the hippocampal CA1 region[24]. The standard deviation of the first latency distribution, a quantitative measure for the synchrony of release, was significantly larger in CCK than in PV interneuron–granule cell synapses (0.95 ± 0.30 ms versus 0.26 ± 0.06 ms; $P < 0.05$; **Fig. 2a–c**). Third, CCK interneuron–granule cell synapses showed a larger proportion of failures of transmission than did PV interneuron–granule cell synapses (18.6 ± 6.3% versus 0.5 ± 0.3%; $P < 0.005$). Fourth, the 20–80% rise time of evoked IPSCs was longer in CCK interneuron–granule cell synapses than in PV interneuron–granule cell synapses (0.87 ± 0.08 ms versus 0.53 ± 0.04 ms; $P < 0.001$; **Fig. 2a–c**), consistent with a more distal location of CCK terminals on the dendrites of granule cells (**Fig. 1c**). In contrast, the weighted IPSC decay time constant was almost identical in the two types of synaptic connection (20.1 ± 0.8 ms versus 20.0 ± 1.1 ms; $P > 0.5$; **Fig. 2c**).

To examine short-term dynamics of synaptic transmission, we evoked gamma-frequency (50 Hz) bursts of ten action potentials in the presynaptic neuron[12] (**Fig. 2d–f**). Both CCK interneuron synapses and PV interneuron synapses showed marked depression during repetitive stimulation; the extent of depression quantified by the ratio $IPSC_{10}$ / $IPSC_1$ was 0.20 ± 0.04 in CCK interneuron–granule cell synapses (13 pairs) and 0.19 ± 0.02 in PV interneuron–granule cell synapses (21 pairs; **Fig. 2f**). However, the onset of depression was slower in CCK interneuron–granule cell synapses than in PV interneuron–granule cell synapses (time constant of 85.6 ms versus 34.8 ms).

Asynchronous release in CCK interneuron–granule cell synapses

In immunocytochemically identified CCK interneuron–granule cell synapses, evoked IPSCs were observed both during and after the train of presynaptic action potentials, suggesting substantial asynchronous transmitter release (**Figs. 2d** and **3a**). We therefore aimed to determine the time course of release by deconvolution[25,26]. To distinguish asynchronous quantal release from spillover of transmitter[27], we performed a nonstationary fluctuation analysis of the postsynaptic current that followed the train[16,28] (**Fig. 3b**). The slope of the variance-mean relation for the current after the train, a measure of the amplitude of the contributing elementary events, was 33.1 ± 3.9 pA (13 CCK interneuron–granule cell pairs). This amplitude was ~30-fold larger than the current through a single $GABA_A$ receptor channel[29,30], arguing for asynchronous release but against spillover. To test the possibility of desensitization of postsynaptic $GABA_A$ receptors[29], we plotted the amplitude of asynchronous events against time after the train (**Fig. 3c**,**d**). If desensitization has a major role, IPSC amplitudes should be smaller at early times than at later times after the train. However, none of the pairs tested showed such a correlation, arguing against desensitization.

To quantify the relative contribution of asynchronous release during and after bursts of action potentials in CCK interneuron–granule cell synapses, we deconvolved average IPSCs from putative quantal IPSCs[25,26] (**Fig. 3e**,**f**; see Methods). Asynchronous release during the train of presynaptic action potentials was determined 15–20 ms after each presynaptic stimulus. Asynchronous release after the train was measured in non-overlapping 5-ms time intervals after the train. **Figure 3e** shows the synchronous component of release and **Figure 3f** the asynchronous components during and after the train. For a 50-Hz train of ten action potentials, the mean relative contributions of synchronous release, asynchronous release during the train and asynchronous release after the train in CCK interneuron–granule cell

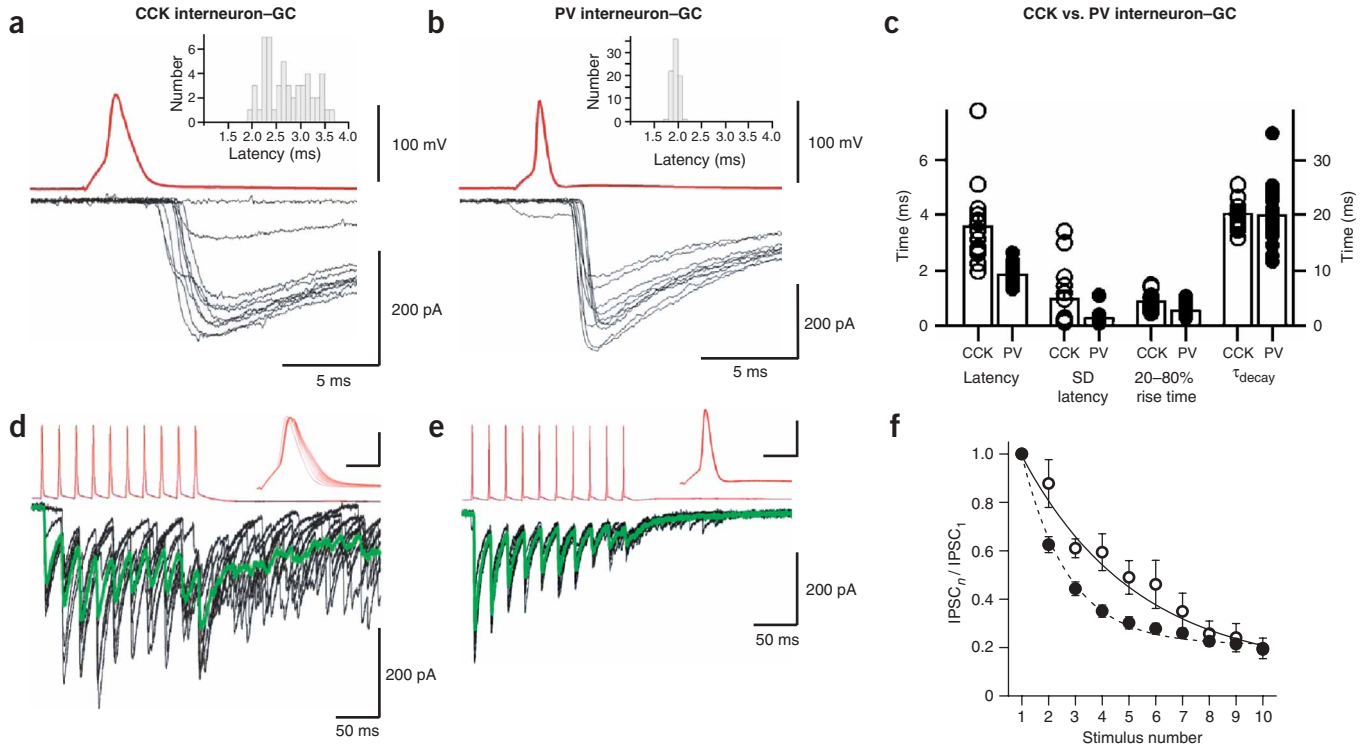

Figure 2 Output synapses of CCK interneurons and PV interneurons differ in basic properties of GABA release. (**a**,**b**) Superimposed IPSCs (black) evoked by single presynaptic action potentials (red) in a CCK interneuron–granule cell (GC) pair (**a**) and a PV interneuron–granule cell pair (**b**). Insets: histograms of IPSC latency. (**c**) Comparison of latency, standard deviation of latency as a measure of temporal precision of release, 20–80% rise time and amplitude-weighted mean decay time constant of IPSCs (τ_{decay}) for CCK interneuron–granule cell pairs versus PV interneuron–granule cell pairs. Right ordinate applies to decay time constant and left ordinate to other parameters. (**d**,**e**) Superimposed IPSCs (black) evoked by trains of ten action potentials (red) in a CCK interneuron–granule cell pair (**d**) and a PV interneuron–granule cell pair (**e**). Green: average IPSCs. Insets: presynaptic action potentials aligned to the stimulus onset at expanded time scale (scale bars: 2 ms, 50 mV). Note action potential broadening in the CCK interneuron (**d**), but constant action potential duration in the PV interneuron (**e**), which may be due to differential expression of voltage-gated K^+ channels[50]. Ten superimposed traces in **a**,**b**,**d**,**e**. (**f**) Onset of multiple-pulse depression of IPSCs during a 50-Hz train of ten action potentials is slower in CCK interneuron–granule cell synapses (open circles) than in PV interneuron–granule cell synapses (filled circles). Mean ratio of $IPSC_n$ / $IPSC_1$, plotted against the numerical index of the stimulus within the train. Curves correspond to exponential functions + offset fitted to the data points.

synapses were 26.6 ± 3.2%, 25.4 ± 2.4% and 48.1 ± 2.9% (13 pairs; 22 ± 2 °C). Thus, with a 50-Hz train of ten action potentials, asynchronous release dominated over synchronous release at CCK interneuron synapses. Asynchronous release decayed with an average time constant of 295 ± 26 ms, indicating that CCK interneuron output synapses can generate long-lasting inhibition (**Fig. 3f**).

Synchronous release in PV interneuron–granule cell synapses

A very different picture emerged in immunocytochemically identified PV interneuron–granule cell synapses (**Fig. 4**). Analysis of the time course of release by deconvolution showed that for 50-Hz bursts of ten action potentials, synchronous release dominated over asynchronous release. **Figure 4a** illustrates the synchronous component of release and **Figure 4b** shows the asynchronous components of release during and after the train. In PV interneuron–granule cell synapses, asynchronous release rate increased slowly during the train of ten action potentials, in contrast to CCK interneuron–granule cell synapses, where asynchronous release rate increased very steeply, reaching a half-maximal value at approximately four action potentials (**Fig. 4c**). In PV interneuron–granule cell pairs, the initial rate of asynchronous release directly after the train of ten action potentials was much smaller (mean rate, 0.016 quanta ms^{-1} versus 0.082 quanta ms^{-1}; $P < 0.001$; **Fig. 4e**, left) and the decay time constant was markedly faster than in CCK interneuron–granule cell pairs (mean τ, 76 ms versus 295 ms; $P < 0.001$; **Fig. 4e**, center). In contrast, the apparent quantal amplitude was similar at the two synapses (mean amplitude, 49.7 pA versus 33.1 pA; $P > 0.5$; **Fig. 4e**, right). Finally, the relative contributions of asynchronous release during and after the train were much smaller in PV interneuron– than in CCK interneuron–granule cell pairs (11.8 and 5.8% for PV interneurons versus 25.4 and 48.1% for CCK interneurons; $P < 0.001$ **Fig. 4d**,**f**). Thus, the two types of GABAergic synapses differed substantially in both extent and time course of asynchronous release.

Presynaptic Ca^{2+} channels in CCK and PV interneurons

Previous studies have suggested that different types of interneurons express different types of presynaptic Ca^{2+} channels[31,32]. However, the Ca^{2+} channel subtype has not been correlated with the expression of immunocytochemical markers. Furthermore, it is unknown whether synchronous and asynchronous release depend on the same type(s) of presynaptic Ca^{2+} channels. We therefore explored the effects of peptide Ca^{2+} channel blockers on GABA release[33] (**Fig. 5**). In CCK interneuron synapses, 1 μM ω-conotoxin GVIa, a selective blocker of N-type channels, completely inhibited both the peak amplitude of the first IPSC in the train and the integral under the current after the train ($IPSC_{1,\omega\text{-cono}}$ / $IPSC_{1,control}$ = 2.2 ± 0.8% and $\int IPSC_{\omega\text{-cono}}$ / $\int IPSC_{control}$ = 0.1 ± 0.2%, respectively, measured 17 min after toxin

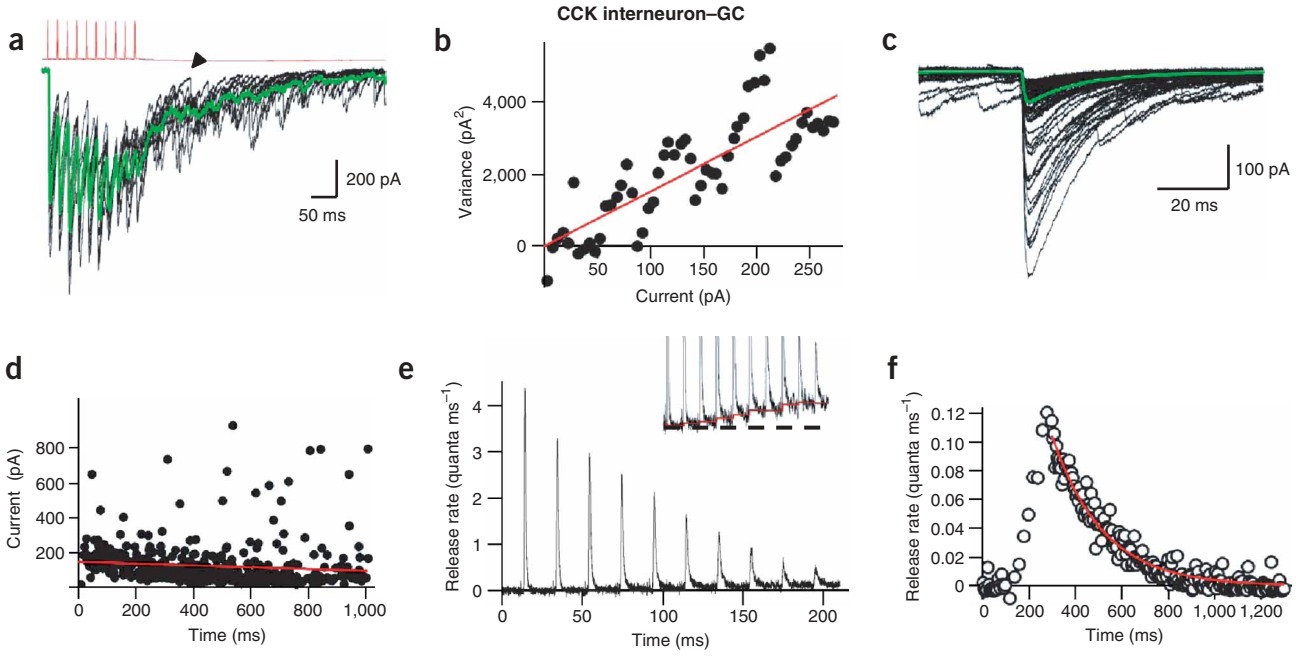

Figure 3 Asynchronous release at CCK interneuron output synapses. (**a**) Superimposed IPSCs (black) evoked by train of ten presynaptic action potentials (red) in an immunocytochemically identified CCK interneuron–granule cell (GC) pair. Green curve: average IPSC. Arrowhead: time period in which the current almost reaches the baseline value. (**b**) Nonstationary fluctuation analysis of current after a train of action potentials. Variance was corrected for baseline noise, plotted against mean current and averaged in 5-pA bins. Red line was obtained by linear regression. (**c**) Single synaptic events underlying asynchronous release after the train. IPSCs were detected with a template fit algorithm, aligned by their rising phase and averaged; 71 events are shown superimposed. Green curve: average IPSC scaled by the median peak amplitude. (**d**) Peak amplitude of asynchronous IPSCs versus time; $t = 0$ indicates end of the action potential train. Red line: linear regression to data points (correlation coefficient 0.11). (**e**) Time course of release during a train of ten presynaptic action potentials in a CCK interneuron–granule cell pair determined by deconvolution. Inset: vertically expanded version of time course of release (low-pass filtered at 2 kHz, partially truncated for clarity). Red line: asynchronous release determined as the mean release rate 15–20 ms after the onset of each stimulus. (**f**) Time course of asynchronous release during and after the train determined by deconvolution. Red curve: result of exponential fitting to the decay phase (time constant $\tau = 218$ ms). All data were obtained from the same CCK interneuron–granule cell pair.

application; three pairs; **Fig. 5a**,**b**). Likewise, 1 μM ω-conotoxin GVIa blocked compound IPSCs evoked by stimulation of inner molecular layer axons (activating CCK terminals; **Fig. 1c**), whereas 500 nM ω-agatoxin IVa, a selective blocker of P/Q-type Ca^{2+} channels, had no effect (**Fig. 5b**, inset). These results indicate that both synchronous and asynchronous release from CCK interneuron synaptic terminals is exclusively mediated by N-type Ca^{2+} channels.

In contrast, in PV interneuron synapses 500 nM ω-agatoxin IVa nearly abolished both the first IPSC in the train and the integral under the current after the train ($IPSC_{1,\omega\text{-aga}} / IPSC_{1,control} = 5.2 \pm 2.2\%$ and $\int IPSC_{\omega\text{-aga}} / \int IPSC_{control} = 3.9 \pm 11.6\%$, respectively; three pairs; **Fig. 5c**,**d**). Whereas 500 nM ω-agatoxin IVa blocked compound IPSCs evoked by stimulation of granule cell layer axons (activating PV terminals; **Fig. 1c**), 1 μM ω-conotoxin GVIa had no effect (**Fig. 5d,** inset). These results indicate that release from PV interneuron synaptic terminals is exclusively mediated by P/Q-type Ca^{2+} channels. Thus, different types of Ca^{2+} channels mediate transmitter release at CCK and PV interneuron synapses, whereas each type of Ca^{2+} channel can support both synchronous and asynchronous release.

Differential effects of Ca^{2+} chelators

To test whether a long-lasting increase in the global Ca^{2+} concentration in the presynaptic terminals[17] underlies asynchronous release in CCK interneuron output synapses, we examined the effects of EGTA-AM, a membrane-permeant Ca^{2+} chelator with a slow binding rate for Ca^{2+} (refs. 34–36; **Fig. 6**). Bath application of 100 μM EGTA-AM blocked asynchronous release in CCK interneuron–granule cell synapses, as quantified by the integral under the average current after the train ($\int IPSC_{EGTA\text{-}AM} / \int IPSC_{control} = 10.7 \pm 7.0\%$; measured 25 min after onset of the application; four pairs; **Fig. 6a**,**b**). EGTA-AM also accelerated the decay of the average synaptic current after the train in CCK interneuron–granule cell synapses (decay time constant: 306 ± 92 ms in control; 64 ± 24 ms after EGTA-AM; $P < 0.1$). In PV interneuron–granule cell synapses, EGTA-AM similarly reduced asynchronous release after the train ($\int IPSC_{EGTA\text{-}AM} / \int IPSC_{control} = 20.4 \pm 14.9\%$; six pairs; **Fig. 6c**) but had no effect on the decay time constant ($\tau = 39 \pm 7$ ms in control versus 33 ± 5 ms after EGTA-AM; $P > 0.5$). Thus, after application of EGTA-AM the decay time course of the current after the train became comparable in the two synapses. These results indicate that a long-lasting presynaptic Ca^{2+} transient drives asynchronous release in CCK interneuron synapses, whereas the Ca^{2+} transient in PV interneuron synapses seems to be shorter.

Notably, 100 μM EGTA-AM also affected synchronous release in CCK interneuron–granule cell synapses, reducing the peak amplitude of the first IPSC in the train to 6.8 ± 3.8% of the control value (four pairs; **Fig. 6a**,**b**,**d**). In contrast, EGTA-AM had no significant effect on synchronous release in PV interneuron–granule cell synapses ($IPSC_{1,EGTA\text{-}AM} / IPSC_{1,control} = 117.7 \pm 17.2\%$; six pairs; **Fig. 6c**,**d**). We therefore further tested the effects of BAPTA-AM, a Ca^{2+} chelator with a ~100-fold faster binding rate for Ca^{2+} (refs. 35,36). However, 100 μM BAPTA-AM led to only a moderate reduction of synchronous release at PV interneuron–granule cell synapses ($IPSC_{1,BAPTA\text{-}AM}$ /

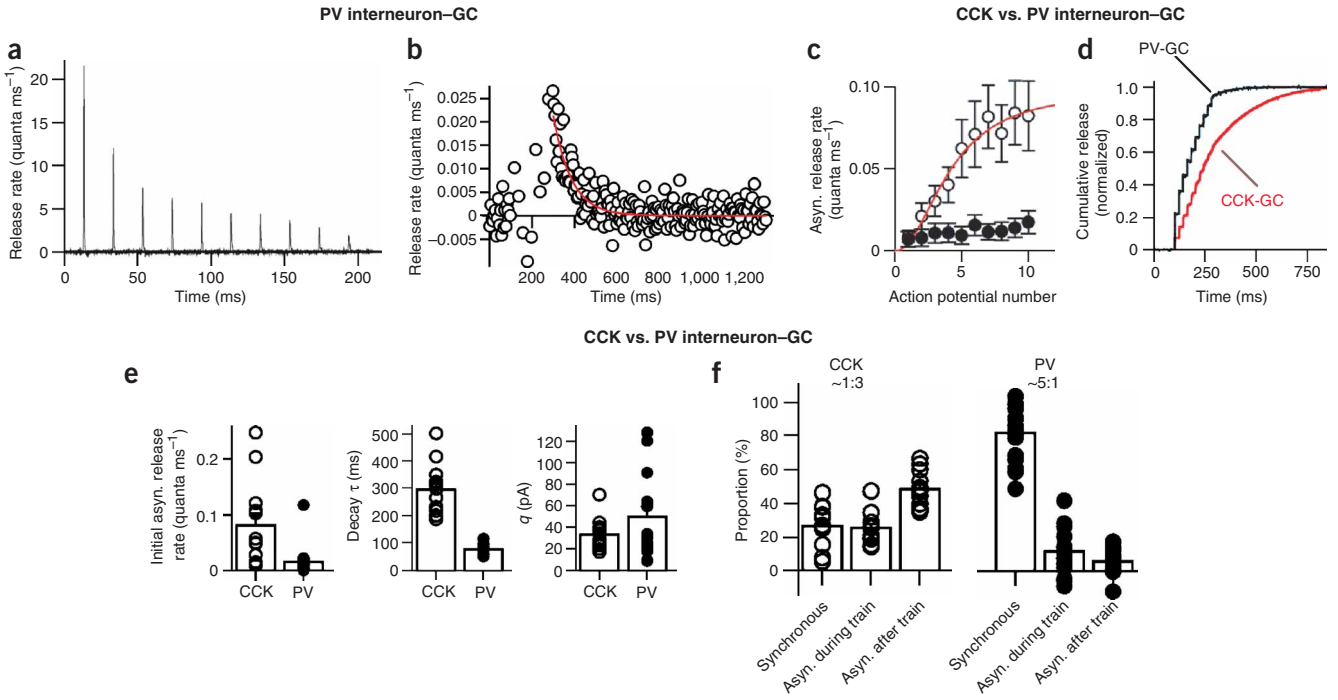

Figure 4 Ratio of asynchronous to synchronous release in CCK and PV interneuron–granule cell synapses. (**a**) Time course of release during a train of ten presynaptic action potentials in an immunocytochemically identified PV interneuron–granule cell (GC) pair determined by deconvolution. (**b**) Time course of asynchronous release during and after the train in the same pair. Red curve: exponential function fitted to the decay phase (time constant $\tau = 85$ ms). (**c**) Asynchronous release during the train for CCK interneuron–granule cell pairs (open circles) and PV interneuron–granule cell pairs (filled circles). Red curve represents the function $f_1(n)$ (see Methods) fitted to the CCK interneuron–granule cell pair data ($k_{0.5} = 4.1$; $h = 2.1$). (**d**) Normalized cumulative release plotted against time for the CCK interneuron–granule cell pair shown in **Figure 3** and the PV interneuron–granule cell pair shown in **a**,**b**. (**e**) Summary bar graph of initial asynchronous release rate after the train (left), decay time constant of asynchronous release (center) and apparent quantal amplitude (q, right) in immunocytochemically identified CCK and PV interneuron–granule cell pairs. Asynchronous release was quantified by deconvolution, and q was determined by nonstationary fluctuation analysis. (**f**) Relative contribution of synchronous release, asynchronous release during the train and asynchronous release after the train in CCK and PV interneuron–granule cell synapses. Ratios of synchronous over asynchronous release are indicated above. In all experiments, a 50-Hz train of ten presynaptic action potentials was used.

$IPSC_{1,control} = 63.9 \pm 4.3\%$; seven pairs; **Fig. 6d**). As CCK interneuron output synapses are markedly more sensitive to Ca^{2+} chelators than PV interneuron output synapses, our results suggest a larger diffusional distance between the Ca^{2+} source and the Ca^{2+} sensor that triggers release in CCK interneuron terminals[34–37].

Pattern dependence of asynchronous release

Hippocampal interneurons *in vivo* fire in bursts, with variable number and frequency of action potentials[38]. We therefore analyzed the dependence of asynchronous release on these parameters in both CCK and PV interneuron output synapses. Single presynaptic action potentials and bursts of three, six and ten action potentials at frequencies of 50, 142 or 200 Hz were applied, and asynchronous release was quantified by deconvolution analysis (**Fig. 7**). In CCK interneuron–granule cell pairs, asynchronous release after the train increased supralinearly with the number of action potentials (**Fig. 7a**,**c**). In contrast, the initial rate of asynchronous release measured directly after the train saturated with increasing action potential number (**Fig. 7d**). Additionally, the decay of asynchronous release after the train was markedly dependent on action potential number (**Fig. 7e**; time constants 58, 44, 125 and 295 ms for one, three, six, and ten action potentials, respectively; $P < 0.001$). Thus, the increase of asynchronous release with action potential number was caused by both an increase in the initial release rate and a slowing of the decay of asynchronous release. In contrast, in PV interneuron output synapses, the extent of asynchronous release was markedly smaller (**Fig. 7c**,**d**) and the decay was much faster (**Fig. 7e**).

In CCK interneuron output synapses, asynchronous release was independent of the stimulation frequency (50 and 142 Hz; $P > 0.5$). In PV interneuron output synapses, asynchronous release slightly increased with stimulation frequency (50, 142 and 200 Hz, $P < 0.05$; ten action potentials in all cases); however, the substantial difference between CCK and PV interneurons was apparent in all conditions (**Fig. 7c–e**).

Asynchronous release at near-physiological temperature

Finally, we tested whether asynchronous release occurred at higher temperature (**Fig. 8**). At 34 ± 2 °C, asynchronous release from CCK interneuron terminals after ten action potentials at 50 Hz was preserved (**Fig. 8a**). The maximal rate of asynchronous release at 34 °C was not significantly different from that at 22 °C (0.067 quanta ms^{-1} versus 0.082 quanta ms^{-1}; $P > 0.5$; 4 and 13 pairs, respectively; **Fig. 8c**). However, asynchronous release decayed more rapidly at 34 °C (decay τ, 139 ms versus 295 ms; $P < 0.1$; **Fig. 8d**). As a consequence, the proportion of asynchronous release during and after the train was smaller at 34 °C than at 22 °C (46% versus 73%; **Fig. 8e**). However, this reduction could be overcome by increasing action potential frequency from 50 to 100 Hz and action potential number from 10 to 25 (asynchronous release 83%; **Fig. 8f**). Under all conditions tested, the substantial difference between CCK and PV interneuron output

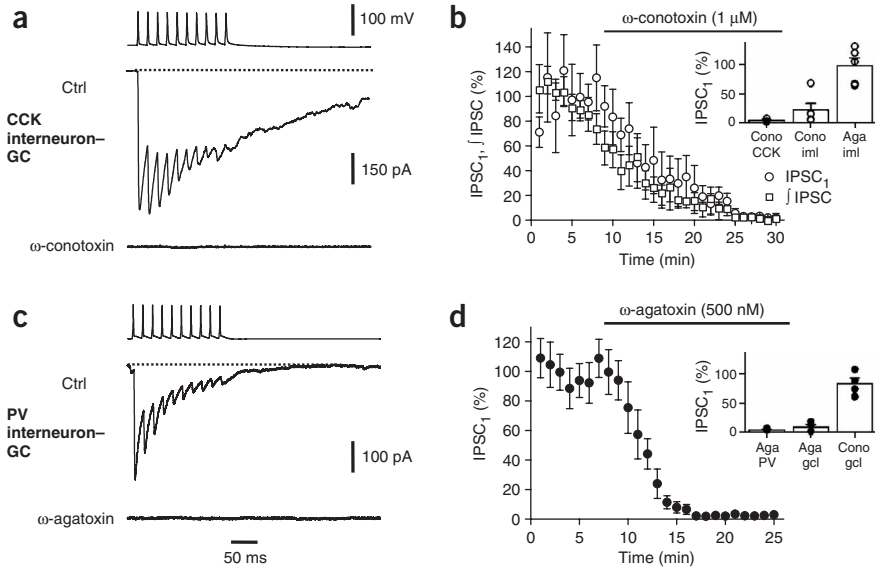

Figure 5 Different Ca^{2+} channels mediate transmission in CCK and PV interneuron synapses. (**a**) ω-conotoxin GVIa (1 μM) blocks synaptic transmission at CCK interneuron–granule cell (GC) synapses. Upper trace: train of ten presynaptic action potentials; lower traces: average IPSCs under control conditions and after application of the toxin (at the end of the application period). (**b**) Plot of peak current of the first IPSC in the train ($IPSC_1$; open circles) and the integral of the current after the train (70–310 ms after the end of the train; open squares) against recording time (three pairs). Bar indicates time of application of toxin. Inset: summary of normalized unitary IPSC amplitude in CCK interneuron–granule cell pairs in the presence of ω-conotoxin ('cono'), together with normalized amplitude of compound IPSCs evoked by extracellular axon stimulation in the inner molecular layer (iml) in the presence of 1 μM ω-conotoxin and 500 nM ω-agatoxin IVa ('aga'). (**c**) ω-agatoxin IVa (500 nM) blocks synaptic transmission at PV interneuron–granule cell synapses. Upper trace: train of ten presynaptic action potentials; lower traces: average IPSCs under control conditions and after application of the toxin. (**d**) Plot of $IPSC_1$ against recording time (four pairs). Inset: summary of normalized unitary IPSC amplitude in PV interneuron–granule cell pairs in the presence of ω-agatoxin, together with normalized amplitude of compound IPSCs evoked by extracellular axon stimulation in the granule cell layer (gcl) in the presence of 500 nM ω-agatoxin and 1 μM ω-conotoxin. IPSC traces are averages of 30–40 sweeps.

synapses was preserved ($P < 0.05$; **Fig. 8e,f**). At 34 °C, approximately five action potentials were sufficient to induce asynchronous release from CCK terminals (5% of maximal release rate at 3.4 and 1.8 action potentials and half-maximal release rate at 7.7 and 4.5 action potentials, for ten action potentials at 50 Hz and 25 action potentials at 100 Hz, respectively; **Fig. 8g**).

Hippocampal interneurons *in vivo* fire bursts of action potentials at theta frequency during exploration[38]. Although the natural firing pattern of CCK interneurons in the dentate gyrus remains to be determined, we tested whether a theta-burst stimulation protocol induced asynchronous release from CCK terminals. At 34 °C, bursts of five action potentials repetitively applied at a frequency of 4 Hz led to profound asynchronous release (**Fig. 8h**) that greatly exceeded asynchronous release evoked by isolated bursts. The same pattern gave similar results in five additional experiments in which compound IPSCs were evoked by stimulation of inner molecular layer axons (data not shown). Thus, asynchronous release from CCK interneuron terminals occurs at near-physiological temperature and with behaviorally relevant stimulation patterns, suggesting that it may generate a presynaptic form of long-lasting inhibition in the brain *in vivo*.

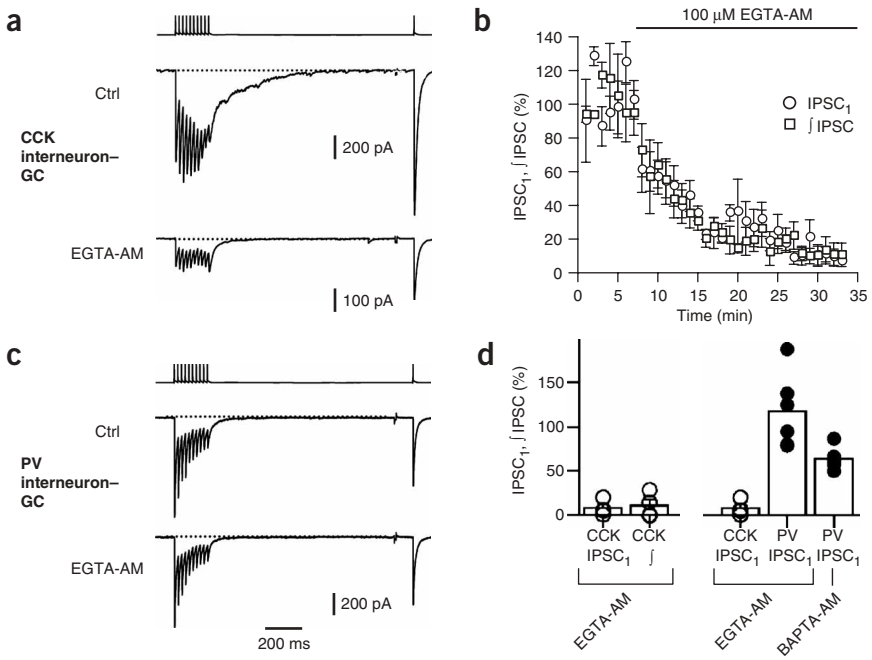

Figure 6 Differential effects of Ca^{2+} chelators on transmitter release in CCK and PV interneuron synaptic terminals. (**a**) Effect of bath application of 100 μM EGTA-AM on evoked IPSCs in CCK interneuron–granule cell (GC) synapses. (**b**) Plot of peak current of the first IPSC in the train ($IPSC_1$; normalized to control) and the integral of the current after the train (100–1,000 ms after the end of the train) against recording time (four pairs). Horizontal bar indicates time of application of EGTA-AM. (**c**) Effect of 100 μM EGTA-AM on evoked IPSCs in PV interneuron–granule cell synapses. (**d**) Summary of the effect of EGTA-AM on synchronous and asynchronous release in CCK interneuron–granule cell synapses (left; four pairs) and comparison of effects of Ca^{2+} chelators on synchronous release (right; EGTA-AM on CCK interneuron–granule cell synapses and EGTA-AM and BAPTA-AM on PV interneuron–granule cell synapses; four, six and seven pairs, respectively). Synchronous release was measured as $IPSC_1$; asynchronous release was quantified as the integral after the train. IPSC traces are averages of 30–50 sweeps.

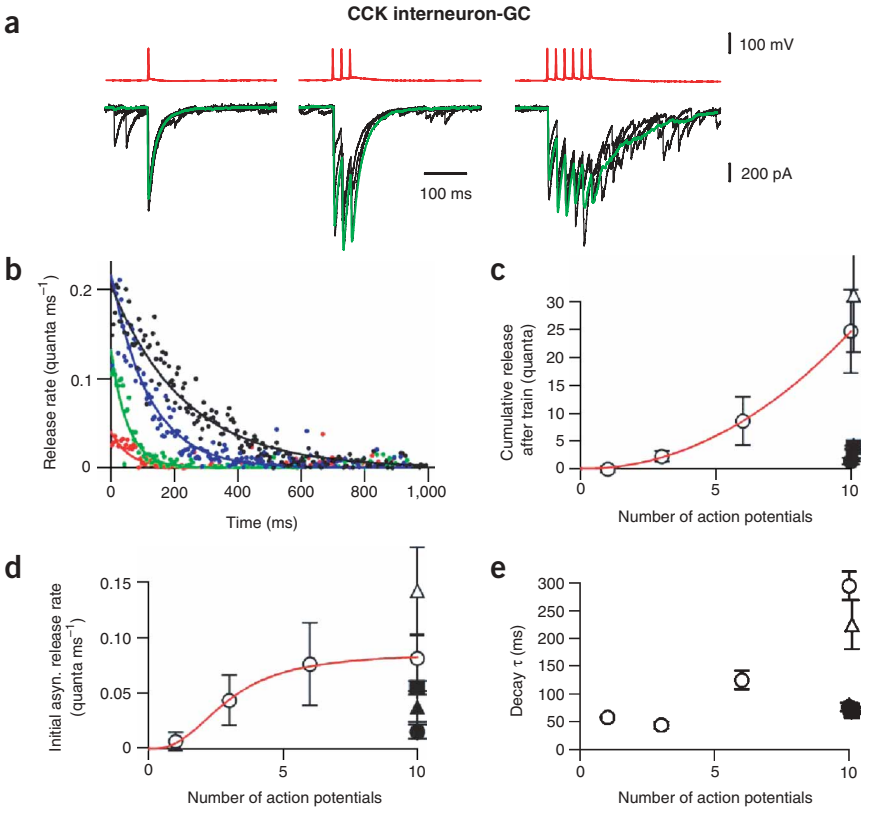

Figure 7 Dependence of asynchronous release from CCK terminals on number and frequency of presynaptic action potentials. (**a**) Superimposed IPSCs (black) evoked by single presynaptic action potentials or trains of three or six action potentials (red) in a CCK interneuron–granule cell pair. Three single sweeps are superimposed; green curve represents average of 25–30 sweeps. (**b**) Time course of asynchronous release after single action potentials or trains of three, six and ten action potentials in same CCK interneuron–granule cell pair as in **a**, obtained by deconvolution analysis (red, green, blue and black, respectively). The superimposed curves represent exponential functions fitted to the data points (time constants (τ) 59, 53, 120 and 232 ms). (**c**–**e**) Asynchronous release after the stimulus train (**c**), initial asynchronous release rate (**d**) and decay time constant of asynchronous release (**e**), plotted against the number of action potentials. Open symbols, CCK interneuron–granule cell pairs (circles: one, three, six and ten action potentials at 50 Hz; triangles: ten action potentials at 142 Hz; seven pairs). Filled symbols, PV interneuron–granule cell pairs (circles: ten action potentials at 50 Hz; triangles: ten action potentials at 142 Hz; squares: ten action potentials at 200 Hz; nine pairs). Triangles and squares were shifted to the right by 0.1 for clarity in **c** and **e**. Red curves represent functions fitted to CCK interneuron–granule cell data (**c**, $f_2(n)$; $h = 2.1$; **d**, $f_1(n)$; $k_{0.5} = 2.9$; $h = 2.6$).

DISCUSSION

These findings indicate that the mechanisms of coupling of action potentials and exocytosis differ substantially between CCK and PV interneuron synapses. CCK interneurons use N-type Ca^{2+} channels (Cav2.2) for transmitter release, whereas PV interneurons rely on P/Q-type channels (Cav2.1). Furthermore, the differential effects of Ca^{2+} chelators suggest that the coupling between the Ca^{2+} channels and the Ca^{2+} sensor of exocytosis is looser in CCK than in PV interneuron output synapses[34–37]. This conclusion fits with the involvement of different types of Ca^{2+} channels in synaptic transmission. In the calyx of Held (at postnatal day 8–10), P/Q-type channels are clustered at active zones, whereas N-type channels are distributed throughout the presynaptic terminals[37]. Likewise, at the cerebellar climbing fiber synapse, release at active zones is controlled by P/Q-type channels, whereas ectopic release is mediated by N-type Ca^{2+} channels[39].

Although the differential effect of EGTA on synchronous release indicates a major difference in the average distance between Ca^{2+} source and sensor at the two synapses, the intracellular concentrations of externally applied Ca^{2+} chelators are unknown; hence, absolute distances are difficult to determine. In cerebellar parallel fiber synapses, bath application of 100 μM EGTA-AM leads to an accumulation of ~10 mM EGTA in presynaptic intracellular compartments (compare **Figs. 5b** and **10a** in ref. 40). If the same intracellular concentration were reached in the terminals of CCK and PV interneurons, the mean distance that Ca^{2+} diffuses before it was captured by EGTA would be $\lambda = \sqrt{D_{Ca} / (k_{on} * [EGTA]_{free})} \approx 50$ nm, where D_{Ca} is the diffusion coefficient for Ca^{2+}, 220 $\mu m^2\ s^{-1}$; k_{on} is the Ca^{2+} binding rate of EGTA, $10^7\ M^{-1}\ s^{-1}$; and $[EGTA]_{free}$ is the concentration of free EGTA, 10 mM (refs. 35,36). The differential effect of EGTA-AM therefore implies that the distance between Ca^{2+} source and sensor is >50 nm in CCK interneurons but <50 nm in PV interneurons, which would also be consistent with the slightly longer synaptic latencies in CCK interneuron synapses (**Fig. 2c**). Thus, Ca^{2+} 'microdomains' may trigger exocytosis in CCK interneuron terminals, whereas 'nanodomains' could be involved in PV interneuron terminals.

CCK interneuron output synapses show an approximately fivefold larger maximal asynchronous release rate, a longer duration of asynchronous release and a several-fold larger ratio of asynchronous to synchronous release than do PV interneuron output synapses. What are the underlying molecular mechanisms? Asynchronous release may be related to the loose ('microdomain') coupling between Ca^{2+} source and sensor, as suggested for facilitation at neocortical synapses[34]. Loose coupling would reduce synchronous release, whereas tight coupling would increase it. Thus, loose coupling will increase the ratio of asynchronous to synchronous release, but it alone is not sufficient to explain the large absolute rates and the long duration of asynchronous release at CCK interneuron synapses (**Fig. 4e**)[36].

Alternatively, asynchronous release may be driven by a long-lasting presynaptic Ca^{2+} transient[17,40]. This mechanism would explain the high absolute rate and the long duration of asynchronous release in CCK interneurons. The hypothesis of a long-lasting presynaptic Ca^{2+} transient in CCK terminals is strongly supported by the effects of EGTA-AM, which reduces both the extent and duration of asynchronous release (**Fig. 6a**). The assumption of a long-lasting Ca^{2+} transient in CCK interneurons also fits with the possibility of peptide release from large dense core vesicles, which are thought to require long-lasting Ca^{2+} elevations for fusion[41].

The difference in the time course of presynaptic Ca^{2+} transients could be generated by different Ca^{2+} buffering in the two classes of interneurons. CCK interneurons seem to lack the expression of specialized Ca^{2+}-binding proteins, as indicated by the minimal overlap of immunoreactivity for CCK with immunoreactivities for PV

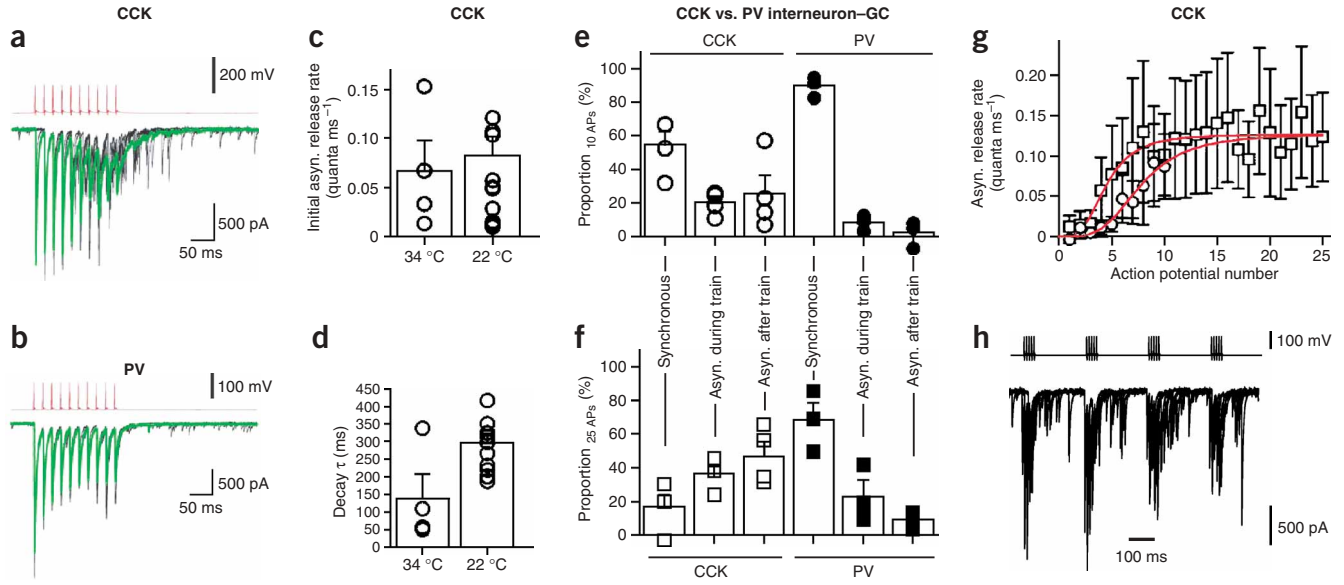

Figure 8 Asynchronous release from CCK interneuron synapses at near-physiological temperature and with theta-burst stimulation patterns. (**a**,**b**) Superimposed IPSCs (black) evoked by trains of ten presynaptic action potentials (red) at 50 Hz in a CCK interneuron–granule cell (GC) pair (**a**) and a PV interneuron–granule cell pair (**b**) at 34 °C. Five single sweeps are superimposed. Green curve: average of 25–30 sweeps. (**c**,**d**) Initial asynchronous release rates (**c**) and decay time constants of asynchronous release in CCK interneuron–granule cell pairs (**d**) at 34 °C and 22 °C (4 and 13 pairs, respectively). Trains of ten presynaptic action potentials at 50 Hz in all cases. (**e**,**f**) Relative contribution of synchronous release, asynchronous release during trains and asynchronous release after trains of ten presynaptic action potentials at 50 Hz (**e**) and 25 presynaptic action potentials at 100 Hz (**f**; four and three pairs, respectively). (**g**) Asynchronous release during the train for CCK interneuron–granule cell pairs for ten presynaptic action potentials at 50 Hz (circles) and 25 presynaptic action potentials at 100 Hz (squares). Red curves represent the function $f_1(n)$ ($k_{0.5} = 7.7$, $h = 3.6$ for ten action potentials at 50 Hz; $k_{0.5} = 4.5$, $h = 3.3$ for 25 action potentials at 100 Hz; a constrained to the same value). (**h**) Overlay of five consecutive 1-s traces of IPSCs from a CCK interneuron–granule cell pair during the onset of theta-burst stimulation (five stimuli at 100 Hz applied at a repetition frequency of 4 Hz). In five additional experiments in which compound IPSCs were evoked by stimulation of inner molecular layer axons, the same procedure gave similar results. All data were obtained at 34 ± 2 °C unless otherwise noted.

(**Fig. 1c**), calretinin and calbindin in the hippocampus (S.H., unpublished observations)[2]. In contrast, PV provides a major contribution to the Ca^{2+} buffering capacity in neurons expressing this Ca^{2+}-binding protein[42,43]. Our results are consistent with the view that the lack of PV facilitates asynchronous release in CCK interneurons, whereas PV expression suppresses asynchronous release in PV interneurons by slow binding of Ca^{2+} (but see ref. 43).

Alternatively, asynchronous release could be generated by a high-affinity Ca^{2+} sensor of exocytosis[44,45]. The primary candidate molecule for the Ca^{2+} sensor seems to be synaptotagmin. Thus, low-affinity synaptotagmins (such as synaptotagmin 1, 2 and 3) trigger synchronous release, whereas high-affinity synaptotagmins (such as synaptotagmin 5, 6, 7, 9 and 10) may drive asynchronous release[44,45]. Among all synaptotagmins, synaptotagmin 7 seems to be the most suitable candidate for asynchronous release from CCK interneurons because it shows the highest Ca^{2+} affinity[44] and the slowest disassembly kinetics of Ca^{2+}-synaptotagmin-membrane complexes ($\sim 10\ s^{-1}$ at 15 °C)[45]. Although a scenario in which the decay of asynchronous release is governed exclusively by the rate of Ca^{2+} unbinding from synaptotagmin is unlikely, as EGTA-AM reduces both the extent and duration of asynchronous release, a contribution of high-affinity Ca^{2+} synaptotagmins to asynchronous release in CCK interneurons cannot be excluded. Thus, asynchronous release from CCK interneurons may be generated by the combination of multiple molecular mechanisms.

The different release properties of the output synapses of CCK and PV interneurons define a functional division of labor in the dentate gyrus network. On the basis of the location of somata and dendrites, it is likely that the two types of interneurons are integrated in both feed-forward and feedback inhibitory microcircuits. However, whereas PV interneurons are highly sensitive to changes in activity and generate phasic output[11,46], CCK interneurons summate activity and provide a long-lasting inhibitory signal. Thus, inhibition mediated by PV interneurons will be generated at the onset of repetitive activity, whereas inhibition involving CCK interneurons will be activated at later times. This will contribute to dynamic routing of inhibition either to the perisomatic region near the action potential initiation site or to the proximal dendrites of postsynaptic granule cells where excitatory synapses terminate[46]. Thus, routing may occur at the level of both input synapses[46] and output synapses (as we found here) of different interneuron subtypes.

CCK interneurons generate a long-lasting, fluctuating inhibitory signal at granule cell proximal dendrites. What is the computational significance of such an inhibitory signal? Previous studies have suggested that both fluctuating inhibition and balanced excitatory-inhibitory synaptic input preferentially change the gain of input-output relations, whereas tonic inhibition is more efficient in controlling the offset[7,47] (P.J., unpublished simulations in granule cells). As CCK interneurons provide a fluctuating output and also regulate the balance between excitation and inhibition, they could serve to implement an efficient gain control mechanism. Thus, CCK interneurons may enable multiplicative operations in the neuronal network of the dentate gyrus. As a corollary, neuromodulators (such as endocannabinoids, serotonin or acetylcholine), which preferentially affect CCK interneurons or their output synapses[22,32,48], may shift between offset and gain control and thus between additive and multiplicative information processing.

METHODS

Paired recording. Transverse 300-μm-thick hippocampal slices were cut from brains of 19- to 22-d-old Wistar rats using a custom-built or a commercial vibratome (DTK-1000, Dosaka). The animals were killed by decapitation, in accordance with national and institutional guidelines. For storage of slices, a solution containing 87 mM NaCl, 25 mM $NaHCO_3$, 10 mM glucose, 75 mM sucrose, 2.5 mM KCl, 1.25 mM NaH_2PO_4, 0.5 mM $CaCl_2$ and 7 mM $MgCl_2$ was used. For experiments, slices were superfused with a solution containing 125 mM NaCl, 25 mM $NaHCO_3$, 25 mM glucose, 2.5 mM KCl, 1.25 mM NaH_2PO_4, 2 mM $CaCl_2$ and 1 mM $MgCl_2$ (equilibrated with 95% O_2/5% CO_2). In a subset of paired recording experiments, 10 μM CNQX and 20 μM R-CPP were added to the bath solution.

Patch pipettes were pulled from borosilicate glass tubing. The intracellular solution used for the presynaptic interneuron contained 135 mM potassium gluconate, 20 mM KCl, 0 or 0.1 mM EGTA, 2 mM $MgCl_2$, 2 mM Na_2ATP, 0.5 mM GTP, 5 mM phosphocreatine, 10 mM HEPES and 0.1% or 0.2% biocytin. The intracellular solution used for the postsynaptic granule cell contained 110 mM KCl, 35 mM potassium gluconate, 10 mM EGTA, 2 mM $MgCl_2$, 2 mM Na_2ATP, 10 mM HEPES, 0.5 or 1 mM QX-314 and 0.1% or 0.2% biocytin. The pipette resistance was 2 to 4 MΩ. Two Axopatch 200A amplifiers (Axon Instruments) were used for simultaneous recording from pre- and postsynaptic neurons. The presynaptic neuron was held in the current-clamp mode (I-Clamp fast) and stimulated by brief current pulses (1.5 ms, 2–3 nA). Single stimuli or trains of 3–25 stimuli at 50–200 Hz were applied every 10–30 s. The postsynaptic cell was held in the voltage-clamp configuration at −80 mV with series resistance (R_S) compensation (~70–90%, lag ~20 μs; R_S before compensation 4–20 MΩ). Signals were filtered at 10 kHz (4-pole low-pass Bessel filter) and digitized at 20 kHz using a CED 1401plus interface (Cambridge Electronic Design). Pulse generation and data acquisition were performed using either FPulse (U. Fröbe, Physiologisches Institut, Freiburg) running under Igor (version 5.01) or commercial programs (CED) on a PC. Peptide toxins were applied with a recirculation system (volume ~15 ml, flow 1.5 ml min^{-1}, equilibrated with O_2/CO_2). In these experiments, bovine serum albumin (0.001%) was added to the bath solution before and during the experiment to prevent adsorption of the peptides to surfaces and 3 μM phenol red was added to monitor the pH. ω-conotoxin-GVIa and ω-agatoxin-IVa were from Bachem, and EGTA-AM and BAPTA-AM were from Molecular Probes. EGTA-AM and BAPTA-AM stock solutions were prepared in dimethylsulfoxide (DMSO) and diluted in physiological saline directly before the experiment (final concentration of 0.1% DMSO). The recording temperature was 22 ± 2 °C in the majority of experiments and 34 ± 2 °C in a subset (**Fig. 8**). For control measurements, compound IPSCs were evoked in the presence of 10 μM CNQX and 20 μM R-CPP or 50 μM D-2-amino-5-phosphonopentanoic acid by extracellular stimulation of presynaptic axons of CCK interneurons in the molecular layer and axons of PV interneurons in the granule cell layer using glass pipettes (200-μs stimulus duration, 5–10 V stimulus amplitude, 2–4 MΩ resistance).

Post-hoc immunocytochemistry. After recording, slices were fixed with 4% paraformaldehyde in phosphate-buffered solution (PBS; 0.1 M, pH 7.3). After wash with PBS, slices were incubated with 10% goat serum for 1 h and subsequently with a primary monoclonal antibody against either CCK (mouse, CURE/Digestive Diseases Research Center, University of California, Los Angeles, 1:2,000; #9303) or PV (mouse, Swant, 1:5,000–1:10,000; #235) in PBS containing 5% goat serum and 0.2 or 0.3% triton X-100 for 20–24 h at 22 °C. The secondary antibody (goat anti-mouse-Alexa 568, 1:500, Molecular Probes) was applied together with Alexa 488-conjugated avidin-D (Molecular Probes) in PBS and 0.3% triton X-100 for 6–10 h at 22 °C and thereafter overnight at 4 °C. After wash, slices were embedded in Prolong Antifade (Molecular Probes). Control experiments in which the primary antibody was omitted gave no labeling. Likewise, control experiments in which an excess of exogenous antigen was added gave either no (CCK) or very weak (PV) labeling. Labeled neurons were examined with a confocal laser-scanning microscope (LSM 510, Zeiss). For double immunolabeling experiments (**Fig. 1c,d**), a rabbit polyclonal antibody against PV (Swant, 1:1,000; PV-28) and a goat secondary antibody (anti–rabbit Alexa 488, 1:500, Molecular Probes) were used.

Data analysis. Data analysis was performed using Stimfit (P.J. and C. Schmidt-Hieber, Physiologisches Institut, Freiburg) or Mathematica 4.1.2 (Wolfram Research). Synaptic latency (steepest point in the rise of the presynaptic action potential to onset of IPSC), rise time (20% to 80% of IPSC peak amplitude), and the proportion of failures were determined for the IPSC following the first stimulus in a 50-Hz train of ten stimuli. The IPSC decay time constant (amplitude-weighted mean of time constants in a double-exponential fit) was determined from a single IPSC evoked 1.2 s after the train. To quantify multiple-pulse depression, traces were averaged and the amplitude of each IPSC in a train was measured from the baseline directly preceding the rising phase. To perform nonstationary fluctuation analysis of asynchronous release after the train, ensemble variance and ensemble mean were determined for every time point >20 ms after the tenth presynaptic stimulus from 7 to 100 traces. To minimize the effects of rundown, current variance was determined form the differences of overlapping pairs of traces as $\sigma^2 = \langle \Delta^2 \rangle / 2$, where Δ is the difference current[28]. Values of q represent slopes of variance-mean relations, not corrected by a factor of ~2 according to Campbell's theorem[49] and a factor of $(1 + \text{c.v.}^2)^{-1}$ accounting for quantal variability (where c.v. is the coefficient of variation of quantal amplitudes).

To determine the time course of release[25,26], average unitary IPSCs ($IPSC_{unitary}$) were deconvolved from average quantal IPSCs ($IPSC_{quantal}$) as $F^{-1}[F(IPSC_{unitary}) / F(IPSC_{quantal})]$, where F is the discrete Fourier transform and F^{-1} is the inverse. Putative quantal IPSCs after the train were detected with a template fit algorithm. An optimally shaped template was shifted over the data point by point and a correlation coefficient of >0.75–0.9 (data versus amplitude-scaled template) was used as a criterion for detection. IPSCs with monotonic rise and decay were averaged, and the decay was fitted with the sum of two exponentials. For deconvolution, an idealized waveform with instantaneous rise and double-exponential decay was used. The time constants were set to the fitted values, and the amplitude to the median of the IPSC amplitude distribution. Asynchronous release during a train of action potentials was quantified in time intervals 15–20 ms after each presynaptic stimulus. Asynchronous release after the train was measured in non-overlapping 5-ms time intervals ≥20 ms after the last stimulus. Cumulative asynchronous release during and after the train were obtained by integration of the time course of release. For determining the decay time constant of asynchronous release after one, three or six action potentials in CCK interneuron–granule cell synapses and of asynchronous release after ten action potentials in PV interneuron–granule cell synapses (**Fig. 7e**), only pairs with initial asynchronous release rates above the 50th percentile were analyzed. The relation between asynchronous release and action potential number was fitted with the functions $f_1(n) = a\,[1 + (k_{0.5}/n)^h]^{-1}$ or $f_2(n) = a\,n^h$, where n is action potential number, $k_{0.5}$ is the action potential number corresponding to half-maximal release, h is the exponent and a is a constant.

Values are given as mean ± s.e.m. and error bars in figures also indicate s.e.m. whenever they exceed the size of the symbols. Significance of differences was assessed by nonparametric two-sided Wilcoxon signed rank, Mann-Whitney and Kruskal-Wallis tests at the significance level (P) indicated.

ACKNOWLEDGMENTS

We thank J. Bischofberger for support at the confocal microscope and for many discussions; I. Vida and A. Kulik for help with immunocytochemistry; M. Bartos, J. Behrends, J. Bischofberger, K. Haverkampf and M. Heckmann for reading the manuscript and K. Winterhalter and M. Northemann for excellent technical assistance. Supported by the Deutsche Forschungsgemeinschaft (SFB 505, project C5).

COMPETING INTERESTS STATEMENT

The authors declare that they have no competing financial interests.

Published online at http://www.nature.com/natureneuroscience/
Reprints and permissions information is available online at http://npg.nature.com/reprintsandpermissions/

1. Lisman, J.E. Relating hippocampal circuitry to function: recall of memory sequences by reciprocal dentate–CA3 interactions. *Neuron* **22**, 233–242 (1999).
2. Freund, T.F. & Buzsáki, G. Interneurons of the hippocampus. *Hippocampus* **6**, 347–470 (1996).
3. McBain, C.J. & Fisahn, A. Interneurons unbound. *Nat. Rev. Neurosci.* **2**, 11–23 (2001).

4. Miles, R., Tóth, K., Gulyás, A.I., Hájos, N. & Freund, T.F. Differences between somatic and dendritic inhibition in the hippocampus. *Neuron* **16**, 815–823 (1996).
5. Cobb, S.R., Buhl, E.H., Halasy, K., Paulsen, O. & Somogyi, P. Synchronization of neuronal activity in hippocampus by individual GABAergic interneurons. *Nature* **378**, 75–78 (1995).
6. Buzsáki, G. & Draguhn, A. Neuronal oscillations in cortical networks. *Science* **304**, 1926–1929 (2004).
7. Mitchell, S.J. & Silver, R.A. Shunting inhibition modulates neuronal gain during synaptic excitation. *Neuron* **38**, 433–445 (2003).
8. Holt, G.R. & Koch, C. Shunting inhibition does not have a divisive effect on firing rates. *Neural Comput.* **9**, 1001–1013 (1997).
9. Datyner, N.B. & Gage, P.W. Phasic secretion of acetylcholine at a mammalian neuromuscular junction. *J. Physiol. (Lond.)* **303**, 299–314 (1980).
10. Isaacson, J.S. & Walmsley, B. Counting quanta: direct measurements of transmitter release at a central synapse. *Neuron* **15**, 875–884 (1995).
11. Kraushaar, U. & Jonas, P. Efficacy and stability of quantal GABA release at a hippocampal interneuron–principal neuron synapse. *J. Neurosci.* **20**, 5594–5607 (2000).
12. Hefft, S., Kraushaar, U., Geiger, J.R.P. & Jonas, P. Presynaptic short-term depression is maintained during regulation of transmitter release at a GABAergic synapse in rat hippocampus. *J. Physiol. (Lond.)* **539**, 201–208 (2002).
13. Bartos, M. *et al.* Fast synaptic inhibition promotes synchronized gamma oscillations in hippocampal interneuron networks. *Proc. Natl. Acad. Sci. USA* **99**, 13222–13227 (2002).
14. Goda, Y. & Stevens, C.F. Two components of transmitter release at a central synapse. *Proc. Natl. Acad. Sci. USA* **91**, 12942–12946 (1994).
15. Jensen, K., Lambert, J.D.C. & Jensen, M.S. Tetanus-induced asynchronous GABA release in cultured hippocampal neurons. *Brain Res.* **880**, 198–201 (2000).
16. Otsu, Y. *et al.* Competition between phasic and asynchronous release for recovered synaptic vesicles at developing hippocampal autaptic synapses. *J. Neurosci.* **24**, 420–433 (2004).
17. Atluri, P.P. & Regehr, W.G. Delayed release of neurotransmitter from cerebellar granule cells. *J. Neurosci.* **18**, 8214–8227 (1998).
18. Lu, T. & Trussell, L.O. Inhibitory transmission mediated by asynchronous transmitter release. *Neuron* **26**, 683–694 (2000).
19. Rumpel, E. & Behrends, J.C. Sr^{2+}-dependent asynchronous evoked transmission at rat striatal inhibitory synapses *in vitro*. *J. Physiol. (Lond.)* **514**, 447–458 (1999).
20. Xu-Friedman, M.A. & Regehr, W.G. Presynaptic strontium dynamics and synaptic transmission. *Biophys. J.* **76**, 2029–2042 (1999).
21. Morozov, Y.M. & Freund, T.F. Postnatal development and migration of cholecystokinin-immunoreactive interneurons in rat hippocampus. *Neuroscience* **120**, 923–939 (2003).
22. Freund, T.F. Interneuron diversity series: Rhythm and mood in perisomatic inhibition. *Trends Neurosci.* **26**, 489–495 (2003).
23. Pawelzik, H., Hughes, D.I. & Thomson, A.M. Physiological and morphological diversity of immunocytochemically defined parvalbumin- and cholecystokinin-positive interneurones in CA1 of the adult rat hippocampus. *J. Comp. Neurol.* **443**, 346–367 (2002).
24. Maccaferri, G., Roberts, J.D.B., Szucs, P., Cottingham, C.A. & Somogyi, P. Cell surface domain specific postsynaptic currents evoked by identified GABAergic neurones in rat hippocampus *in vitro*. *J. Physiol. (Lond.)* **524**, 91–116 (2000).
25. van der Kloot, W. Estimating the timing of quantal releases during end-plate currents at the frog neuromuscular junction. *J. Physiol. (Lond.)* **402**, 595–603 (1988).
26. Diamond, J.S. & Jahr, C.E. Asynchronous release of synaptic vesicles determines the time course of the AMPA receptor-mediated EPSC. *Neuron* **15**, 1097–1107 (1995).
27. Hamann, M., Rossi, D.J. & Attwell, D. Tonic and spillover inhibition of granule cells control information flow through cerebellar cortex. *Neuron* **33**, 625–633 (2002).
28. Heinemann, S.H. & Conti, F. Nonstationary noise analysis and application to patch clamp recordings. *Methods Enzymol.* **207**, 131–148 (1992).
29. Jones, M.V. & Westbrook, G.L. Desensitized states prolong $GABA_A$ channel responses to brief agonist pulses. *Neuron* **15**, 181–191 (1995).
30. Brickley, S.G., Cull-Candy, S.G. & Farrant, M. Single-channel properties of synaptic and extrasynaptic $GABA_A$ receptors suggest differential targeting of receptor subtypes. *J. Neurosci.* **19**, 2960–2973 (1999).
31. Poncer, J.C., McKinney, R.A., Gähwiler, B.H. & Thompson, S.M. Either N- or P-type calcium channels mediate GABA release at distinct hippocampal inhibitory synapses. *Neuron* **18**, 463–472 (1997).
32. Wilson, R.I., Kunos, G. & Nicoll, R.A. Presynaptic specificity of endocannabinoid signaling in the hippocampus. *Neuron* **31**, 453–462 (2001).
33. Randall, A. & Tsien, R.W. Pharmacological dissection of multiple types of Ca^{2+} channel currents in rat cerebellar granule neurons. *J. Neurosci.* **15**, 2995–3012 (1995).
34. Rozov, A., Burnashev, N., Sakmann, B. & Neher, E. Transmitter release modulation by intracellular Ca^{2+} buffers in facilitating and depressing nerve terminals of pyramidal cells in layer 2/3 of the rat neocortex indicates a target cell-specific difference in presynaptic calcium dynamics. *J. Physiol. (Lond.)* **531**, 807–826 (2001).
35. Neher, E. Usefulness and limitations of linear approximations to the understanding of Ca^{++} signals. *Cell Calcium* **24**, 345–357 (1998).
36. Meinrenken, C.J., Borst, J.G.G. & Sakmann, B. Calcium secretion coupling at calyx of Held governed by nonuniform channel-vesicle topography. *J. Neurosci.* **22**, 1648–1667 (2002).
37. Wu, L.G., Westenbroek, R.E., Borst, J.G.G., Catterall, W.A. & Sakmann, B. Calcium channel types with distinct presynaptic localization couple differentially to transmitter release in single calyx-type synapses. *J. Neurosci.* **19**, 726–736 (1999).
38. Bragin, A. *et al.* Gamma (40–100 Hz) oscillation in the hippocampus of the behaving rat. *J. Neurosci.* **15**, 47–60 (1995).
39. Matsui, K. & Jahr, C.E. Differential control of synaptic and ectopic vesicular release of glutamate. *J. Neurosci.* **24**, 8932–8939 (2004).
40. Atluri, P.P. & Regehr, W.G. Determinants of the time course of facilitation at the granule cell to Purkinje cell synapse. *J. Neurosci.* **16**, 5661–5671 (1996).
41. Verhage, M. *et al.* Differential release of amino acids, neuropeptides, and catecholamines from isolated nerve terminals. *Neuron* **6**, 517–524 (1991).
42. Schmidt, H., Stiefel, K.M., Racay, P., Schwaller, B. & Eilers, J. Mutational analysis of dendritic Ca^{2+} kinetics in rodent Purkinje cells: role of parvalbumin and calbindin D_{28k}. *J. Physiol. (Lond.)* **551**, 13–32 (2003).
43. Collin, T. *et al.* Developmental changes in parvalbumin regulate presynaptic Ca^{2+} signaling. *J. Neurosci.* **25**, 96–107 (2005).
44. Südhof, T.C. Synaptotagmins: why so many? *J. Biol. Chem.* **277**, 7629–7632 (2002).
45. Hui, E. *et al.* Three distinct kinetic groupings of the synaptotagmin family: candidate sensors for rapid and delayed exocytosis. *Proc. Natl. Acad. Sci. USA* **102**, 5210–5214 (2005).
46. Pouille, F. & Scanziani, M. Routing of spike series by dynamic circuits in the hippocampus. *Nature* **429**, 717–723 (2004).
47. Chance, F.S., Abbott, L.F. & Reyes, A.D. Gain modulation from background synaptic input. *Neuron* **35**, 773–782 (2002).
48. Losonczy, A., Biró, A.A. & Nusser, Z. Persistently active cannabinoid receptors mute a subpopulation of hippocampal interneurons. *Proc. Natl. Acad. Sci. USA* **101**, 1362–1367 (2004).
49. Neher, E. & Sakaba, T. Estimating transmitter release rates from postsynaptic current fluctuations. *J. Neurosci.* **21**, 9638–9654 (2001).
50. Zhang, L. & McBain, C.J. Potassium conductances underlying repolarization and afterhyperpolarization in rat CA1 hippocampal interneurones. *J. Physiol. (Lond.)* **488**, 661–672 (1995).